Chapter 5
Photoluminescence of as-prepared and intentionally Ge- implanted CuGaSe$_2$

Why are we keen on doping CuGaSe$_2$ when we can grow high quality CuGaSe$_2$ films? First of all there is a growing interest and a huge advantage in having both p- and n- types within the same semiconductors. Having both n- and p- type within a semiconductor may lead to preparation of homojunctions which have the advantage of not presenting a lattice mismatch at the interface as do heterojunctions. Secondly, CuGaSe$_2$ compounds have been reported to be p- type for all the compositions, in contrast to CuInSe$_2$ which can be tuned n or p type by varying the composition. Thirdly, many attempts to dope CuGaSe$_2$ with extrinsic elements were not sucessful There is only one reported contribution about n- type conduction in CuGaSe$_2$ [71]. Eventually, a model based on theoretical calculations [38] predicted that n- type conduction cannot be achieved in CuGaSe$_2$ compounds.

In our quest to understand the extrinsic and intrinsic doping mechanisms in CuGaSe$_2$, we investigate in this chapter the intrinsic defects of as- prepared CCSVT CuGaSe$_2$ films and also the extrinsic defects induced by Ge ion implantation into the p- type CuGaSe$_2$ films using photoluminescence spectroscopy. In order to introduce controlled amounts of atoms into semiconductors, three key processes are in general used, namely ion implantation, diffusion of adsorbed species from the surface and dpoing during growth. Ion implantation and diffusion are mostly used because they selectively dope the semiconductor material. However, ion implantation is more advantageous compared to diffusion since its allows a more precise control and reproducibility of dopants and it is carried out at relatively low temperatures. Therefore, ion implantation is a very useful and selective process as the mass separation guarantees that only one ion type is used, but it is also the most reliable method of introducing a known concentration of a spectroscopically pure element into a solid. It is noticeable that ion implantation also has disadvantages since it is expensive, not all the damage can be corrected by annealing, and finally it has a higher impurity content than does diffusion. Section 5.1 focusses on the description of Ge ion implantation and annealing processes carried out for this thesis. The elemental depth profile of Ge into CuGaSe$_2$ films is given in section 5.2. Photoluminescence of the undoped films are presented in section 5.3 and the effect of Ge implantation in films on their photoluminescence spectra is investigated in section 5.4.

5.1 Ge- implantation and annealing process of CuGaSe$_2$

The intentional introduction of impurities is fundamental to controlling the properties of bulk semiconductors and has stimulated many efforts to dope semiconductors. Despite some success, many of these efforts have failed for reasons that remain unclear. The CuGaSe$_2$ films used for ion implantation were deposited onto Mo coated soda lime glass using the deposition conditions described in the table 3.1 and have all the same composition of [Ga]/[Cu] = 1.07.

5.1.1 Simulation of the Ge distribution in CuGaSe$_2$ by SRIM program
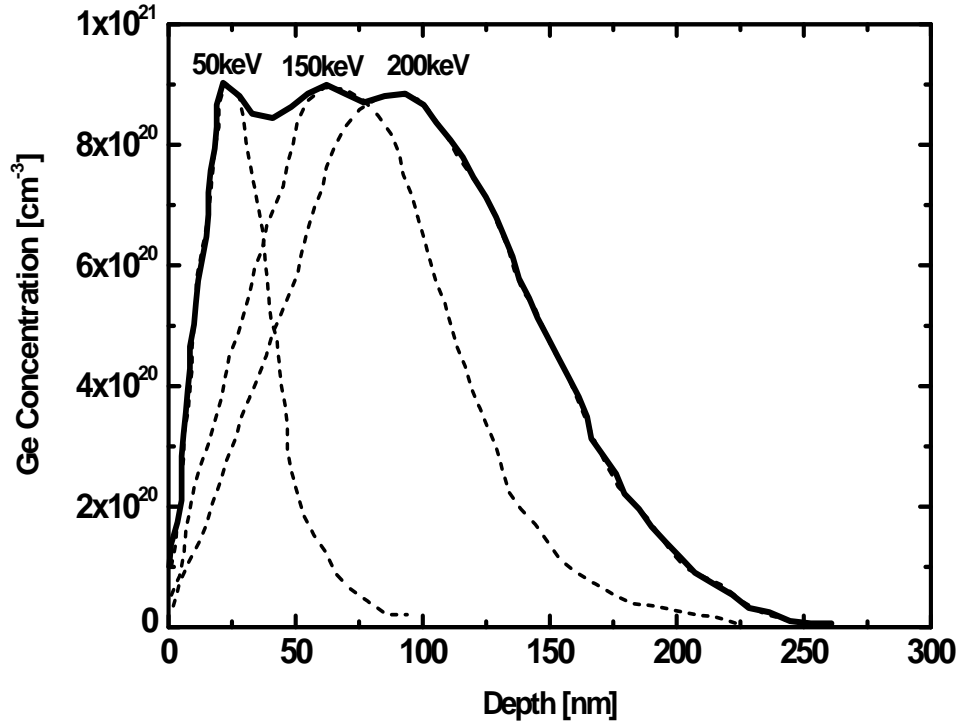
Prior to ion implantation, Monte Carlo simulations were run with the Stopping and Range of Ions in Matter (SRIM 2003) program [70] for the ions injected vertically into the surface of a CuGaSe$_2$ thin film target in order to plan implant dosage with the corresponding energy and therefore predict the penetration depth in the material. Indeed, SRIM is a set of programs which calculate the stopping and range of ions into matter using a quantum mechanical treatment of atomic collisions. Ge ion implantation into three sets of samples (table 5.1) was carried out in two ways:

- Single energy implantation using the kinetic energies of 150 keV and 200 keV at a similar dose of 10^{16}atom/cm^{-2}.

- Three different ion kinetic energies at 50, 150, 200 keV in series and doses of $3\text{x}10^{15}$, $7\text{x}10^{15}$, 10^{16} cm^{-2}. The ion implantation parameters are summarized in table 5.1.

Table 5.1: *Implantation conditions*

Set of samples	Ion	Dose (cm^{-2})	Energy [keV]
#1	Ge	10^{16}	150
#2	Ge	10^{16}	200
#3	Ge	$3\text{x}10^{15}$, $7\text{x}10^{15}$, 10^{16}	50, 150, 200

Figure 5.1 displays the simulated distribution of the Ge ion concentration profile generated by SRIM using threefold energies (set of samples #3) into CuGaSe$_2$ without diffusion effects (grain boundary diffusion and thermal) and sputtering effects such as surface roughing and etching. The estimated penetration depth of Ge ions into the CuGaSe$_2$ films is about 200 nm. One of the main advantages of using three different implantation energies is that a flat Ge depth profile can be achieved. Hence, three accelerating energies, 50, 150, 200 keV were used and the dose at each energy was scaled such that a constant Ge profile can be achieved, accordingly the Ge dose at energies of 50 and 150 keV was reduced with respect to that at the energy of 200 keV by a factor 70% and 30%, respectively. For single energy implantation, the ion distribution under the film surface is a Gaussian function of depth as shown by the dashed line in figure 5.1.

Figure 5.1: *Simulated Ge atom depth profiles in CuGaSe$_2$ (solid line) after 50, 150, 200 keV implantation in series respectively, and Ge profile of the same amount of Ge ions for each energy but with individual implantation (dashed line). The distribution is computed without diffusion effects (thermal diffusion) and without sputtering effects (surface roughening and etching).*
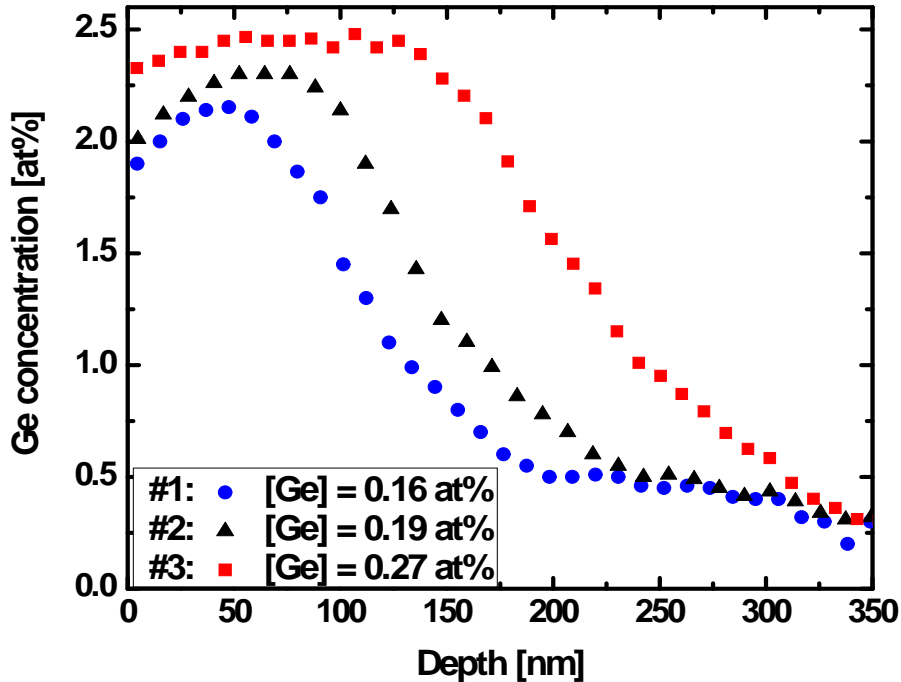
5.1.2 Annealing of Ge implanted CuGaSe$_2$

The accelerated ions in the host semiconductor lattice (as-implanted films) come to rest at the sites which they would likely not occupy under thermodynamic equilibrium conditions. Therefore, in order to enhance the diffusion of the implanted ions and heal the damaged region that always accompanies the implantation, an annealing process is in general required after ion implantation. However during the annealing a combination of several parameters must be taken into account such as annealing time, environment and the cooling process at the end of annealing. The first attempts to anneal Ge implanted CuGaSe$_2$ single crystal were performed by J.H. Schön [71], using RTP (Rapid Thermal Process) at temperatures ranging from 300° C to 400°C and for a duration from 10 to 15 min in the presence of Zn. For the purpose of this thesis, undoped and Ge implanted CuGaSe$_2$ films were annealed in evacuated and sealed quartz ampoules at 450°C for 15 min, in the presence of elements such as (Zn and Cl), in order to remove the compensation [71]. These elements are placed in one

end of the ampoule at T = 450°C and the films to be annealed placed in the other end T = 400°C, and no additional phases were observed after annealing of for the films [72]

5.2 Depth profiling of Ge in CuGaSe₂ by SNMS

Figure 5.2. shows the distribution profile and atomic concentration of Ge atoms implanted into CuGaSe$_2$ thin films extracted from secondary neutral mass spectroscopy (SNMS) spectra. Only the surface region of up to about 250 nm of the CuGaSe$_2$ films is enriched with Ge for incident kinetic energies $E \leqslant 200 \ keV$. From the secondary neutral mass spectroscopy spectra, the overall average atomic Ge concentrations can be estimated by integration within the complete film depth ($\sim 1.7 \mu m$) to be between 0.16 and 0.27 at% as indicated in the inset of the figure 5.2. The depth profile of Ge ions is not different from that of the simulation, only that after annealing, the implanted doping profile is broadened because of many effects such as thermal diffusion after annealing. The measured Ge depth profile is a clear evidence of the presence of Ge near the surface of CuGaSe$_2$ thin films. Obviously, the implantation profiles after annealing of the films are the most homogeneous when three kinetic energies are used.
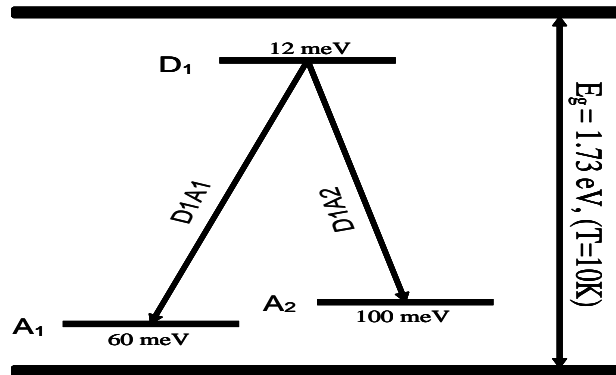

Figure 5.2.: *Depth profile of Ge implanted ions into CuGaSe₂ thin films for the three sets of samples (table 5.1) characterized by secondary neutral mass spectroscopy (SNMS).*

5.3 Photoluminescence of CCSVT as-prepared CuGaSe$_2$ thin films

In this following section, results of defect structures on as-grown CCSVT- CuGaSe$_2$-based thin films by means of photoluminescence are presented. First of all, the evolution of the radiative recombination model in CuGaSe$_2$ is reviewed, followed by the photoluminescence of as-grown CCSVT CuGaSe$_2$ films. The dependence of the excitation intensity with the peak energy is used to determine the sum of ionization energy in the donor acceptor pair recombinations and finally the defect profile of as grown CuGaSe$_2$ is presented. It is shown that there is a correlation between the preparation processes and the defect structure of the CuGaSe$_2$ films.
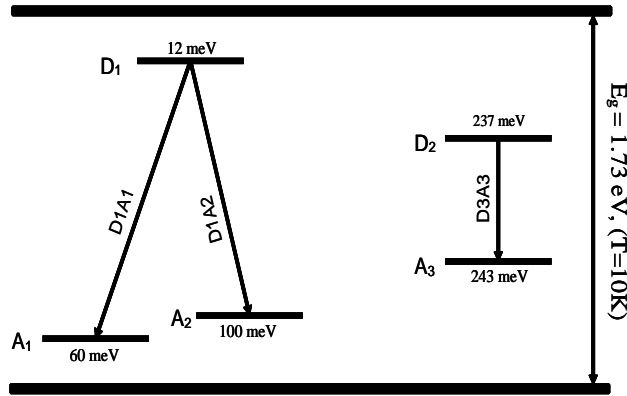
5.3.1 Photoluminescence of CuGaSe$_2$: State of research

Many studies of the point defects and their energy levels in CuGaSe$_2$ have been investigated by a variety of experimental techniques such as photoluminescence [73, 74], and cathodo-luminescence [75]. The first straightforward recombination model of radiative transitions within CuGaSe$_2$ material (crystal and polycrystal) was proposed by Bauchknecht et al [73]. The model consists of two donor- acceptor pair transitions, (D1A1) and (D1A2), with two acceptor levels A_1 and A_2 of ionization energies of E_{A_1}=(60±10) meV and E_{A_2}=(100±10) meV respectively, above the valence band maximum (VBM) and a donor level D_1 of ionization energy E_{D_1}=(12±5) meV below the conduction band minimum (CBM), as shown in figure 5.3.
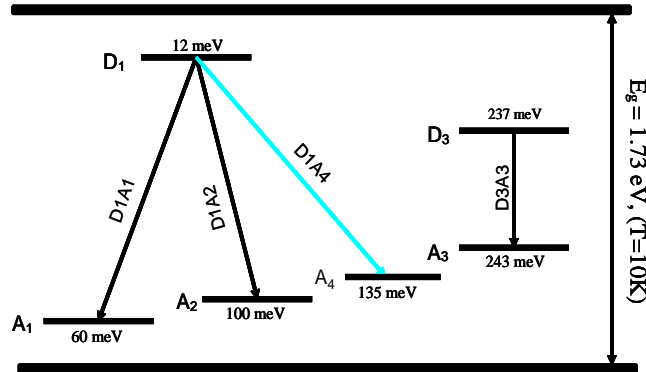

Figure 5.3: *Radiative recombination model of CuGaSe$_2$ (from [73])*

Later on, Meeder *et al* [74] improved the recombination model of CuGaSe$_2$ polycrystalline films and crystals and reported in addition to the defect levels observed by Bauchknecht, new deep donor- acceptor pair transitions (D2A3) with the respective ionization energy of E_{A_3}=(243±20) meV and E_{D_2}=(237±20) meV. Figure 5.4 displays the recombination model proposed by Meeder.

Figure 5.4: *Radiative recombination model of CuGaSe$_2$ (from [74])*

However both models suffered a lack in the assignment of LO-phonon replicas of the donor-acceptor-pair emission (D1A1) transition. Recently a combination of low temperature photoluminescence, and time- and spatially- resolved cathodoluminescence measurements [75] has paved the way and the LO-phonon replicas of the donor- acceptor pair (D1A1) have been rather ascribed to a new donor acceptor transition (D1A4) with a new acceptor ionization energy of E_{A_4} =(135±20) meV. Therefore a new complete recombination model of CuGaSe$_2$ was proposed Siebenttrit *et al* [76] with two donor levels and four acceptor levels as displayed in the figure 5.5.

Figure 5. 5: *Radiative recombination model of CuGaSe$_2$ [76]*

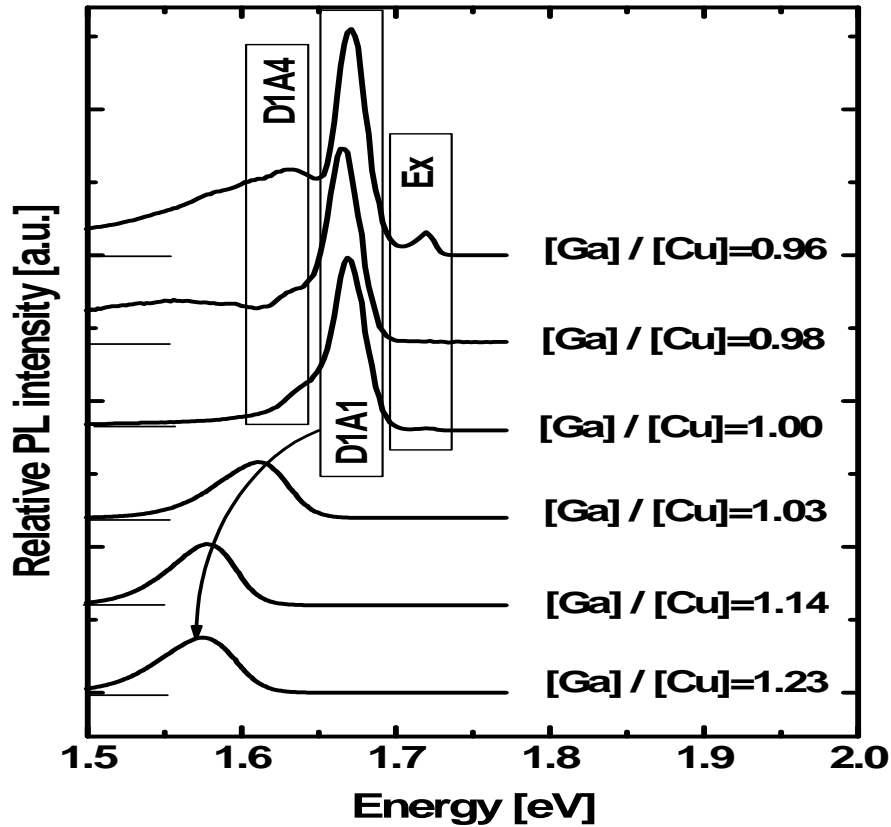## 5.3.2 Photoluminescence of as-grown CCSVT CuGaSe$_2$ thin films

5.3.2.1 Dependence of the photoluminescence spectra on the composition [Ga]/[Cu]:

Figure 5.6 shows the typical photoluminescence emission spectra at 10°K obtained from CuGaSe$_2$ thin films prepared by CCSVT [44] technique with varying compositions. According to the [Ga]/[Cu] ratio, the observed transitions can be ordered as follows:

1. [Ga]/[Cu] >1: Photoluminescence is dominated by a broad and asymmetric transition ascribed to the donor-acceptor pair (D1A1). As the Cu content decreases, the peak

maxima of the D1A1 emission band broadens and shifts towards lower energies (red-shift) as indicated by the arrow in the figure 5.6

2.   [Ga]/[Cu] <1: Photoluminescence spectra show an excitonic emission (Ex) at 1.73eV, the D1A1 emission and the donor- acceptor pair recombination D1A4.

Figure 5.6: *Photoluminescence spectra of polycrystalline CuGaSe$_2$ thin films on Mo coated soda lime glass as a function of the [Ga]/[Cu] ratio at T = 10K and P$_{exc}$ = 50 mW.*

5.3.2.2 **Determination of the ionization energy of the donor- acceptor transition in CuGaSe$_2$ films by means of excitation intensity.**

The determination of the sum of ionization energies of donors (D) and acceptors (A) in a crystal can be achieved through the dependence of the peak energy of the pair-photoluminescence band on excitation intensity [77]. In general, excitation by light produces band-to-band transitions, producing in turn free carriers, which finally are captured by the ionized impurities and transform them into the neutral states following the equation:

$$D^- + A^+ + hv \rightarrow D^0 + A^0 \tag{5.1}$$

The radiative recombination of holes bound to acceptors with electrons bound to donors can occur for both remote or close impurity pairs. Assuming that the pair separation r between donors and acceptors is large enough compared to the radii of the donor and acceptor states, the recombination energies of the pair can be given by:

$$h\nu = E_g - (E_A + E_D) + \frac{e^2}{4\pi\varepsilon\varepsilon_0 r} \tag{5.2}$$

where e is the electronic charge, ε the static dielectric constants, hv is the photon energy of the emission, E_g is the band gap, E_A and E_B are the acceptor and the donor binding energies respectively, and the last term takes into account the electrostatic interaction between electron and hole, bound on the donor and acceptor, respectively. Generally, when r becomes larger ($r \rightarrow \infty$), the emission merges into a broad band. The peak energy of the broad band usually corresponds to the suitable separation pair, which in general depends on excitation intensity and on temperature. In contrast, when r is small, individual pairs may be observed. In the limiting case only the most distant pairs take part in the recombination, so that for $r \rightarrow \infty$, equation 5.2 becomes:

$$hv_\infty = E_g - (E_A + E_D) \tag{5.3}$$

where hv_∞ is the limiting photon energy for distants pairs. Assuming that the semiconductor is not heavily compensated i.e $N_d \ll N_a$, where N_d and N_a are the donor and acceptor concentration respectively, and that the temperature of the semiconductor is low enough so that thermal ionization of donors or acceptors can be neglected, the intensity dependence of a donor- acceptor pair (DAP) recombination band as a function of energy can be determined using the equation 5.4 below [77],

$$I_{PL}(hv) \propto \frac{(hv - hv_\infty)^3}{(hv_B - hv) - (hv - hv_\infty)} \exp\left(\frac{-2(hv_B - hv_\infty)}{hv - hv_\infty}\right) \tag{5.4}$$

where hv is the photon energy of the emission, hv_B and hv_∞ are related by the equation 5.5. The Bohr radius R_B of the shallow hydrogenic impurity is given by:

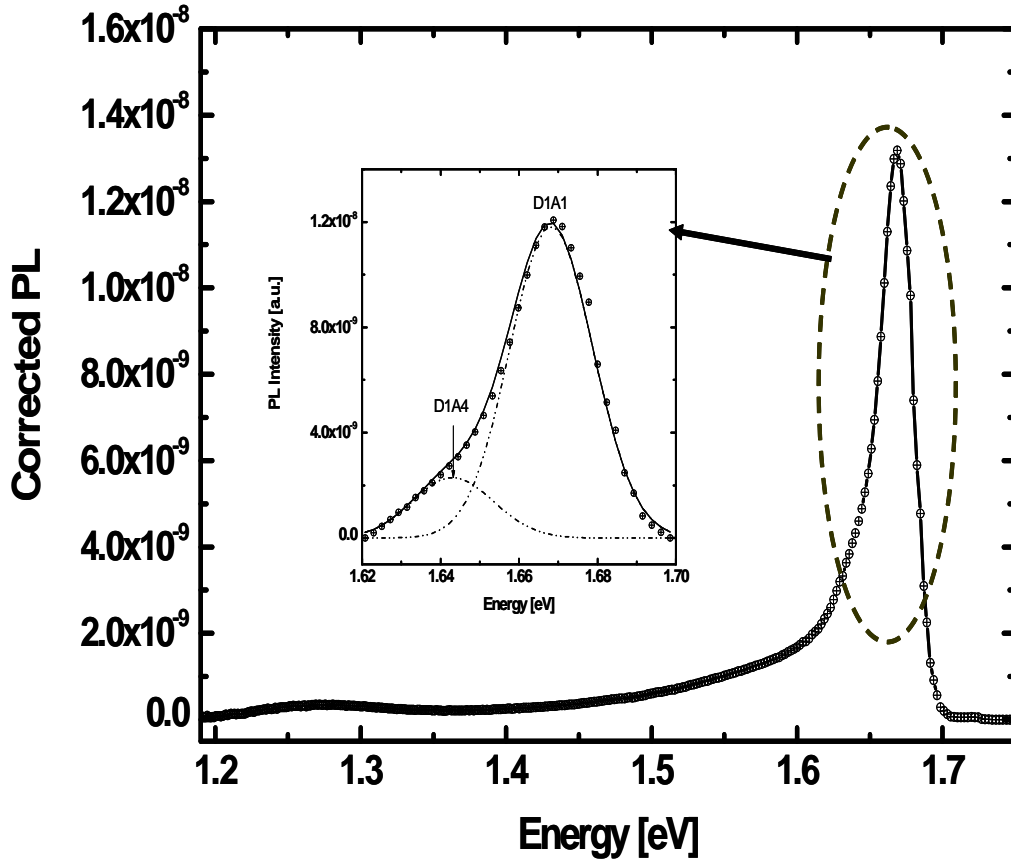$$E_B = hv_B - hv_\infty = \frac{e^2}{4\pi\varepsilon\varepsilon_0 R_B}. \tag{5.5}$$

Hence, the determination of the distant photon energy hv_∞, and the Bohr radius of the hydrogenic shallow impurity R_B by fitting equation 5.4 achieves the determination of the sum of ionization energy of donors and acceptors using equation 5.3.

Figure 5.7 shows the photoluminescence spectrum of a nearly stoichiometric CCSVT as-grown film. Three regions can be defined:

- Photoluminescence between 1.2 and 1.4 eV: a broad donor- acceptor pair transition, D2A3, at hv (D2A3)= 1.27 eV;

- Photoluminescence between 1.6 and 1.7 eV: Two donor- acceptor transitions, D1A and D1A1, at hv (D1A1) = 1.669 eV and hv (D1A4) = 1.644 eV;

- Photoluminescence above 1.7 eV: one free excitonic emission, Ex, at hv (Ex) = 1.725 eV.

Since the transition D1A4 was previously ascribed to the LO phonon of the D1A1 transition, the dependence of the peak energy of the emissions D1A1 and D1A4 on excitation energy are explored to determine the ionization energy of each defect involved in both transitions, assuming that both transitions are donor- acceptor recombinations, and subsequently a comparison of the extracted ionization energies with the literature data is made.

Figure 5.7: *PL spectra of stoichiometric polycrystalline CuGaSe$_2$ thin films at $T = 10K$ and $P_{exc} = 20$ mW. The inset represents the Gaussian fit of the PL peak structure between 1.6 and 1.7 eV.*

The structure of the intermediate energy range between 1.6 eV $<$ hv $<$ 1.7 eV is well fitted using the two Gaussian peaks indicated. Their FWHM and their energy position are summarized in table 5.2. It is worthwhile mentioning that in the previous photoluminescence
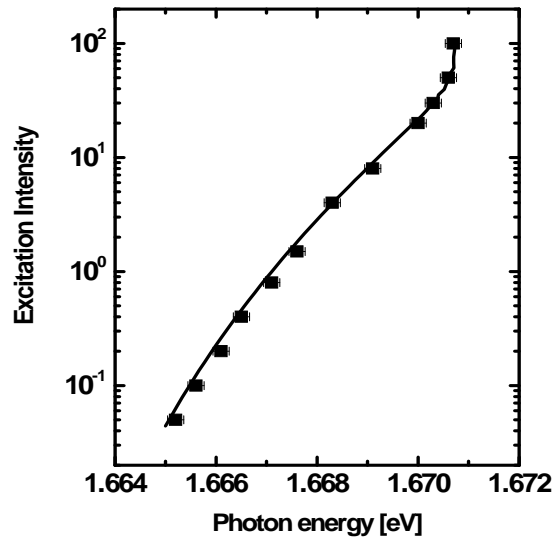
studies, the transition peak at 1.644 eV was erroneously ascribed to a longitudinal optical phonon of the D1A1 pair transition, LO- D1A1 [73, 74].

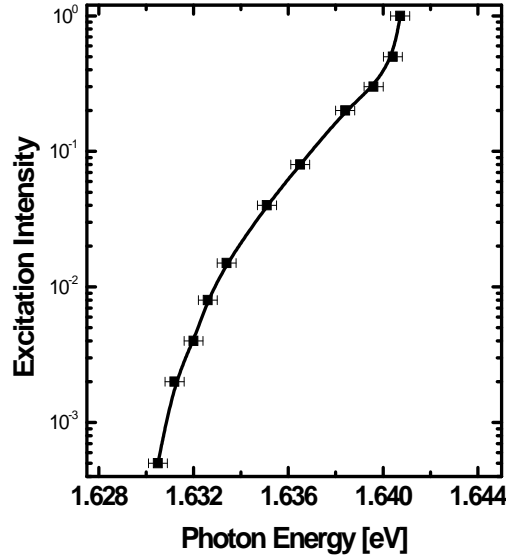**Table 5.2***: Energy and FWHM of the two Gaussian peaks of figure 5.7.*

Gaussian Shape	D1A1	D1A4
hv [eV]	1.644	1.669
$FWHM^*$ [meV]	24.6	24.8

∗FWHM: full width at one half of the maximum height of peaks

Figure 5.8 displays the fitted curves using the experimental data for the dependence of the D1A1 and D1A4 peak energy on the excitation intensity as given by equation 5.4.

(a)

(b)

Figure 5.8: *Fit of equation 5.4 to experimental data for the D1A1 (a) and D1A4 (b) photoluminescence peak in the stoichiometric CCSVT prepared CuGaSe₂ films. The line represents the fitting with parameters hv_∞ and hv_B.*

The computed parameters are summarized in table 5.3, where columns 1 and 2 give the fitting parameters hv_∞, hv_B, column 4 represents the Bohr radius and column 5 is the sum of ionization energies of donor and acceptor levels.

Table 5.3: *Fitting parameters hv_∞, hv_B and the sum of the ionization energies of donor and acceptor levels $E_A + E_D$ as derived from the equation 5.3 with the band gap at $T = 10K$, being $E_g = 1.73$ eV. Bohr radius R_B are determined using fitting parameters. The last column denotes the literature data of $E_A + E_D$.*

Defect	hv_∞ (eV)	hv_B (eV)	E_B (meV)	R_B (Å)	$E_A + E_D$ (meV)	$E_A + E_D$ (meV)
D1A1	1,658±0.01	1,692±0.01	27±10	48	76±10	72 [73]
D1A	1,578±0.01	1,614±0.005	28.4±10	46	155±10	147 [76]

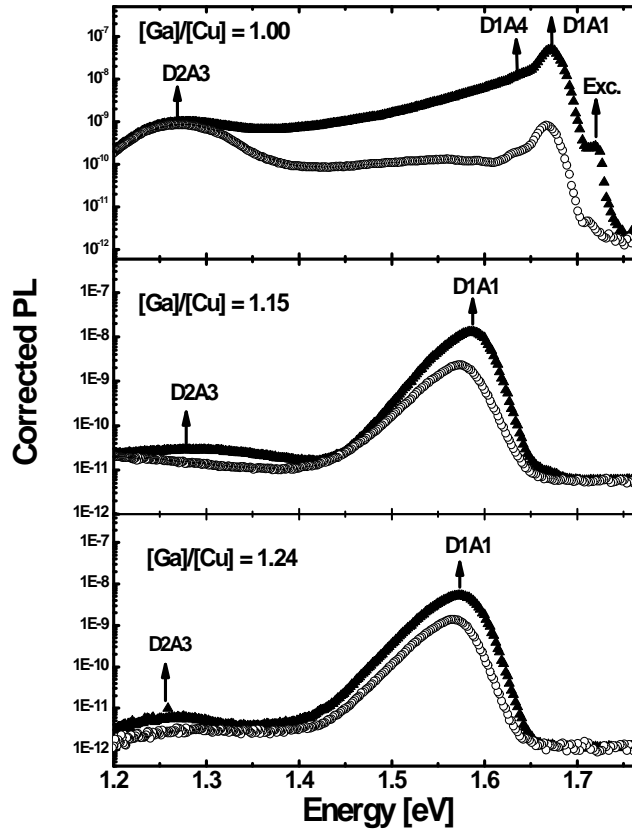Applying the simple hydrogenic model for shallow donor states gives:

$$E_D = \left(\frac{13.6}{\varepsilon^2}\right)\left(\frac{m^*}{m_0}\right) \quad \text{and} \quad \left(\frac{R_H}{R_B}\right) = \varepsilon\left(\frac{m*}{m_0}\right) \tag{5.6}$$

where R_H is the Bohr radius for hydrogen ($R_H = 0.529$ Å), ε and ε_0 are the static dielectric constant of CuGaSe₂ and vacuum dielectric constant, m^*/m_0 is the relative effective mass at the shallow hydrogenic impurity. Taking into account that for CuGaSe₂, $\varepsilon = 11$ [76], and the computed values of the Bohr radius of the donor, R_B, for each donor acceptor pair in

the table 5.3, the donor level is determined to be $E_D = 14\pm10$ meV for D1A4 and 13$\pm$10 meV for D1A1. The donors involved in both transitions are within the error at the same energy level. The energy of the acceptor is involved in the D1A4 transition is obtained to be $E_{A_4} = 134\pm10$ meV. This value is in good agreement with the results obtained by Hall measurements [76, 78, 79],.

5.3.2.3 Defect profiles in CCSVT as-grown CCSVT films

The compared low temperature PL spectra at T = 10 K of the top and back sides of CCSVT-grown CuGaSe$_2$ thin films grown on soda lime glass (SLG) as a function of composition are presented in figure 5.9,
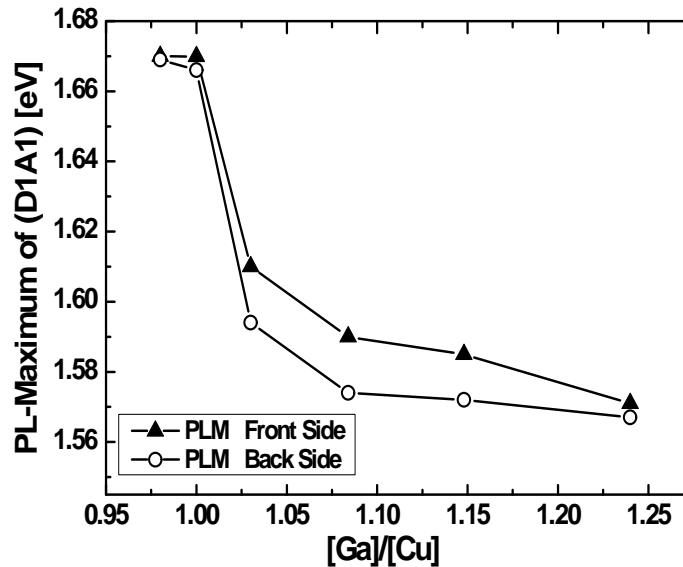

Figure 5.9:. *Logarithmic photoluminescence spectra of the front (full triangles) and back (open circles) sides of the CuGaSe$_2$ thin films on SLG substrates as a function of [Ga]/[Cu] ratio. (T = 10 K, λ = 514.5 nm, P$_{exc}$ = 20 mW).*

The PL spectra of stoichiometric films [Ga]/[Cu] = 1 show a structure which includes an excitonic (Ex) peak at 1.725 eV and the transitions at 1.67 eV, 1.5 eV and 1.27 eV which

correspond to a donor- acceptor pair recombinations *(D1A1), (D1A4)* and *(D2A4),* respectively. The emission line *(D2A3)* at 1.27 eV is caused by the recombination process due to deep defects [74]. These emission lines involve a shallow acceptor A1 ($\backsim$ 60 meV) and deeper acceptors A3 ($\sim$ 240 meV) and A4 ($\sim$ 135 meV). The defect chemical nature of two first acceptors suggested by most of the reports found in the literature is the Cu vacancy (V_{Cu}) [73] and Ga vacancy (V_{Ga}) [74] for the A1 and A3, respectively.

In the PL spectra of films with composition, [Ga]/[Cu] > 1, only *(D1A1)* and *(D2A3)* emission bands are observed. With increasing Ga content these emission bands broaden. In addition, with increasing [Ga]/[Cu] ratio the peak *(D1A1)* shifts to lower energies. This effect is presented also in Ref. [73, 74]. Thus, the *(D1A1)* peak position is an indication of the [Ga]/[Cu] ratio. The more Ga amount contains the sample, the larger red shift expected. From Figure 5.9 we observe that the *(D1A1)* peak in the PL spectra of the CuGaSe$_2$ back side is always positioned at lower energies compared to the position of the same peak at the front side. Therefore, we can conclude that the CuGaSe$_2$ back side contains more Ga than the front side. By plotting the energy peak position of the shallow luminescence *(D1A1)* of both CuGaSe$_2$ sides (front and back) as a function of [Ga]/[Cu] ratio, the evolution of the Ga accumulation near the substrate as well as the defect density have been monitored and are displayed in figure 5.10.

Figure 5.10: *Photoluminescence maximum (PLM) of the shallow defect emission (D1A1) of the front and back sides as a function of [Ga]/[Cu] ratio.*

The energy peak position of the shallow luminescence *(D1A1)* at both front and back sides gradually shifts towards lower energies as Ga increases. Also, with Ga content increase the overall PL intensity goes down. However, the energetic difference ΔPLM between the PL
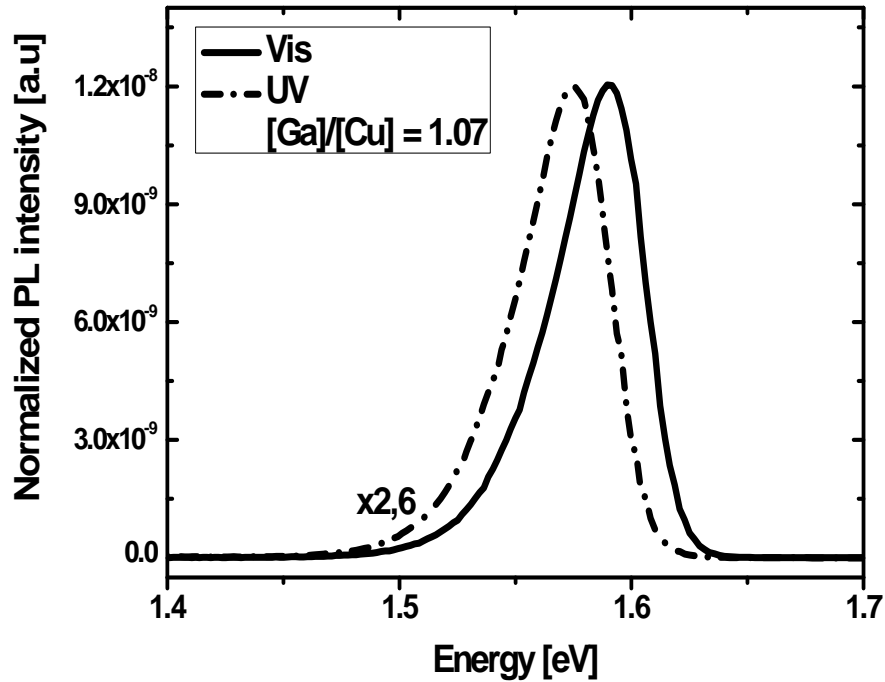
maximum positions of the *(D1A1)* peak at both sides increases and reaches a maximum value at about [Ga]/[Cu] = 1.07. With further [Ga]/[Cu] ratio increase, ΔPLM decreases rapidly to a value of ~ 5 meV, remaining constant up to [Ga]/[Cu] $\backsim$ 1.24. The intensity of the deep defect luminescence *I(D2A3)* decreases significantly, pointing out less Ga vacancies. These results agree well with the CCSVT process stages. In fact, the second CuGaSe₂ growth stage could be regarded as an annealing in GaCl$_x$/H₂Se vapor of the Cu- rich CuGaSe₂ films prepared in the first stage. We may suppose therefore that the Ga defect concentration should decrease with the annealing time. From the above observations, we conclude that V_{Ga} defects are almost homogeneously distributed in the stoichiometric films as well as in samples with [Ga]/[Cu] $\sim$ 1.24. At intermediate compositions a gradient of V_{Ga} defects from the back to front side is formed in the films.

5.4 Effects of Ge- implantation on the photoluminescence of CuGaSe₂ thin films

Photoluminescence (PL) spectra of as- grown , Ge-doped and annealed CCSVT (Chemical closed- space vapor transport) - CuGaSe₂ thin films were excited by the focused beam of an Ar$^+$ laser at the visible (514.5 nm) and ultra- violet (UV) (351.1 nm) lines in order to match the absorption depth with the implant profile.

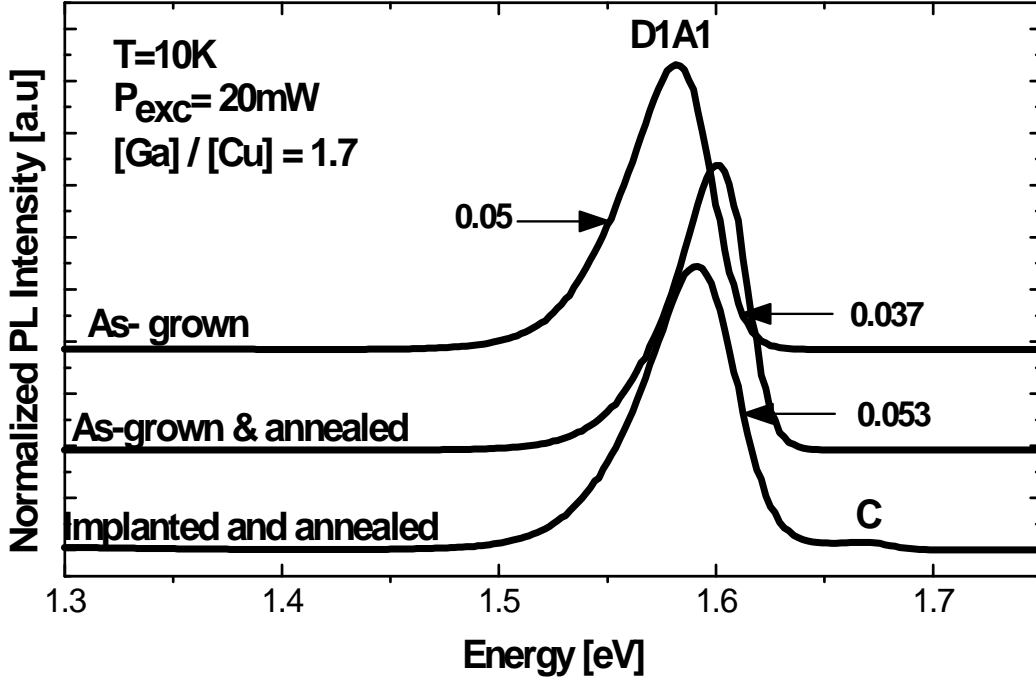### 5.4.1 Comparison of UV and visible photoluminescence spectra of the undoped CGSe thin films

Figure 5.11 displays the UV and visible PL spectra of the undoped and annealed CCSVT-as grown CuGaSe₂ thin films at 10 K. There is not a significant change in the shape of the UV PL spectrum, but only a small shift towards lower energies of $\sim$13 meV is observed with respect to the visible PL spectrum. The shift can be explained by the fact that the surface region of CuGaSe₂ thin films is more Cu- poor than the bulk [80, 81], since UV PL is surface sensitive with a penetration depth of $\sim$150 nm compared to that of the visible with penetration depths to beyond 150 nm.

Figure 5.11: *Visible and UV- PL spectra of CuGaSe$_2$ thin films exhibiting a red-shift of ∼13meV of the Vis PL spectra due the higher surface sensitivity of the UV- PL. (@ 10 K and P$_{exc}$ = 20 mW). The UV-PL spectrum is normalized by a factor 2.6.*

5.4.2 Effect of annealing and Ge- implantation highlighted by visible PL

The aim of this measurement is to point out the effect of each post treatment stage after the growth of the films. After ion implantation, the changes resulting from new defects, such as added impurities, can be all detected by photoluminescence. However, the assignment of specific parameters such as exciton binding energies or ionization energies to the responsible impurity atoms is ambiguous. In order to highlight the effect of the ion implantation, the undoped and Ge- implanted samples were annealed under the same conditions described in subsection 5.1.2. Figure 5.12 shows the spectra of Ge implanted and annealed using threefold energy, as-grown and annealed, and as-grown CuGaSe$_2$ films.

Figure 5.12: *Compared PL spectra of Ge implanted using three kinetic energies, as-grown and implanted, and as-grown films at 10 K and 20 mW measured with the visible line (514.5 nm) of the laser. The arrows indicate the values of the full width at half maximum (FWHM) of the corresponding spectrum*
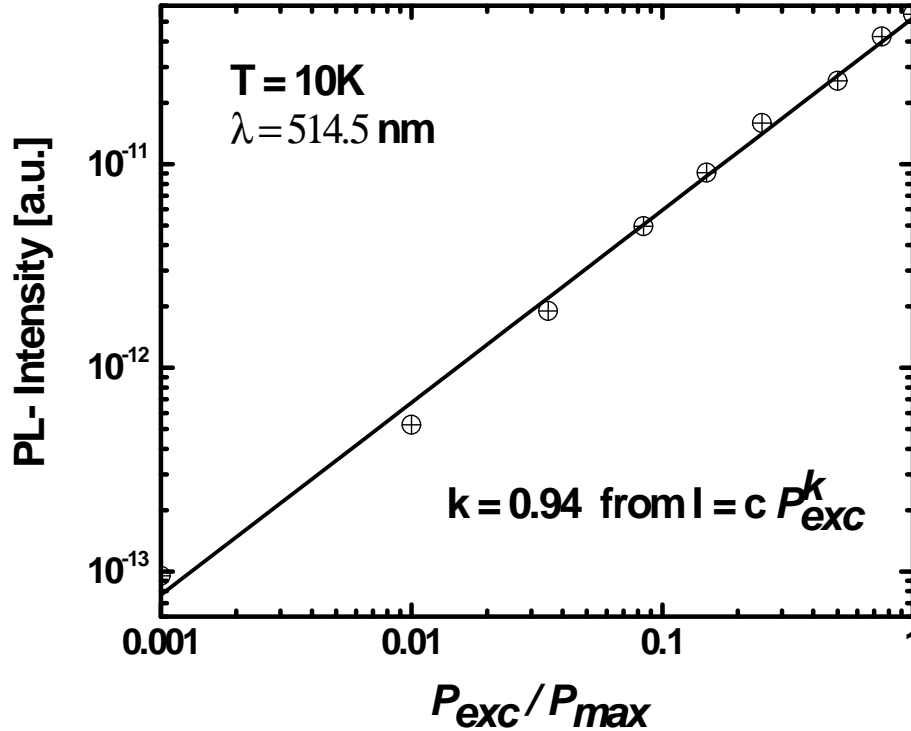
The as-grown, as- grown plus annealed films show almost the same spectral features, namely the broad and asymmetric emission, assigned to the well- known (D1A1) [73] at 1.58 eV. However because of the annealing, the peak is shifted towards higher energy by 20 meV compared to that of the as-grown film. Moreover, the FWHM of all the as- grown films are reduced by 30% after annealing. The Ge- implanted and annealed films exhibit an additional emission feature labelled C appearing at the energy 1.67 eV and a blue shift of ∼10 meV of the D1A1 energy peak position with respect to that of the as-grown film The new feature C has been analyzed by using different power excitation of the laser according to the power law [82]:

$$I_{PL} \propto P_{exc}^{k} \tag{5.7}$$

Where I_{PL} represents the PL intensity, P_{exc}^{k} the excitation power of the laser and k a constant. For excitation with photons of energy exceeding the band gap energy, E_g, the coefficient k is generally $1 < k < 2$ for the free (EX) and bound (BX) exciton emission and $k \leqslant 1$ for

free-to-bound (FB) and donor-to acceptor pair (DAP) recombination. Figure 5.13 shows the dependence of the PL intensity of the C at 1.67 eV emission with power excitation.

Figure 5.13: *Dependence of PL intensity with excitation intensity of the Ge- implantation related 1.67eV peak emission C at 10 K.*
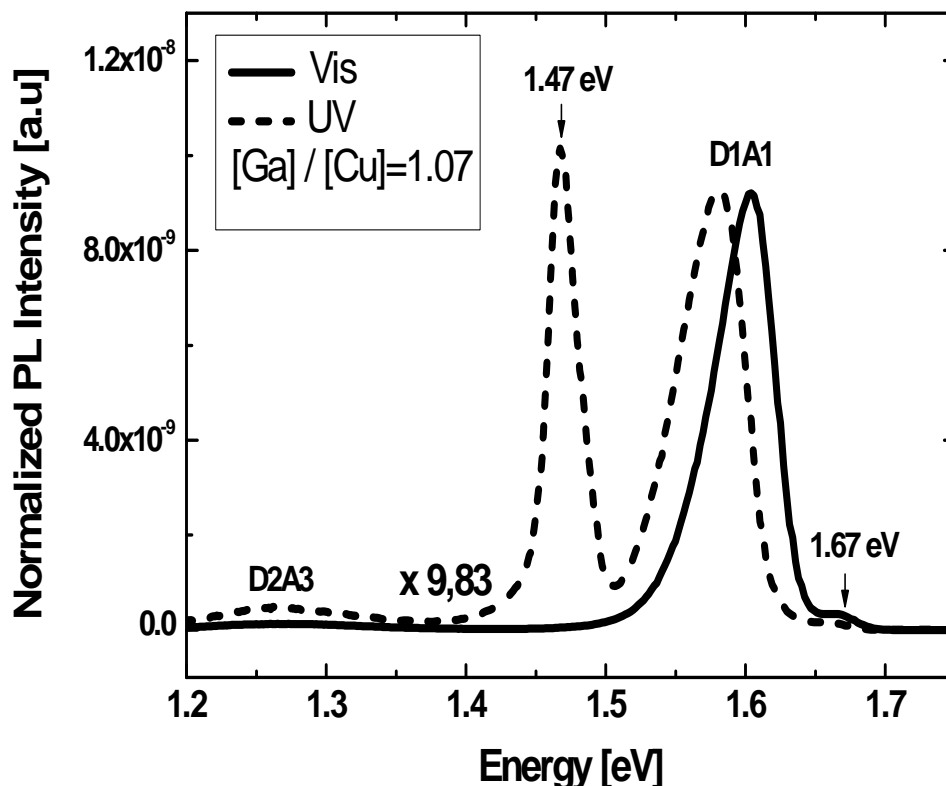
A value of k was obtained to be 0.94. This characteristic is suggestive of either free-to-bound as well as donor- acceptor pair transitions. Already at this point we can state that Ge-implantation creates at least an additional recombination level in the band gap of CuGaSe$_2$.

5.4.3 Effect of Ge implantation on photoluminescence highlighted by UV excitation.

Ge- implanted plus annealed CuGaSe$_2$ thin films were investigated using both visible and UV laser excitations. Figure 5.14 shows a comparison of the UV and vis photoluminescence of the Ge- implanted and annealed CuGaSe$_2$ thin films. The following observations are made:
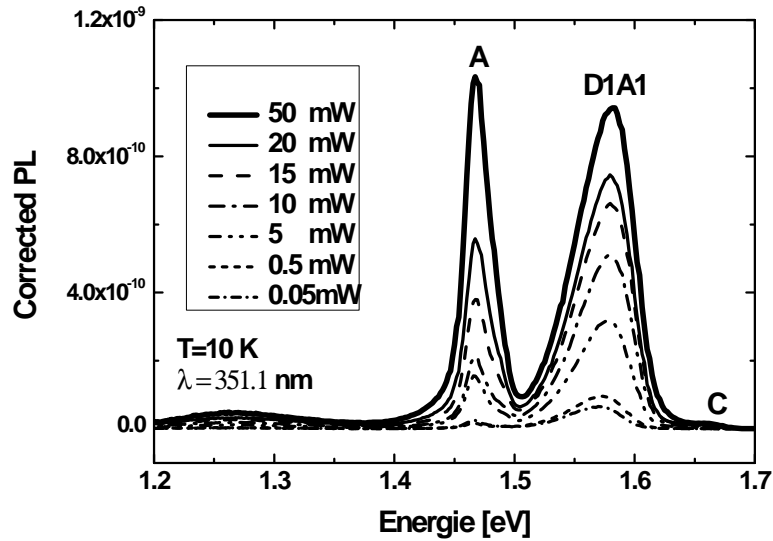
- Vis-PL spectra of the Ge- implanted and thermally treated films exhibits besides the peak emission at 1.604 eV, which is characteristic of donor- acceptor (D1A1) transitions in Cu-deficient material [73, 74], an additional peak emission C at 1.670 eV previously assigned to a new FB or DAP transition.

- UV-PL spectra exhibits in addition to the generally-observed emissions by visible excitation, also a new and remarkable sharp and deep-level emission peaked at 1.47 eV.
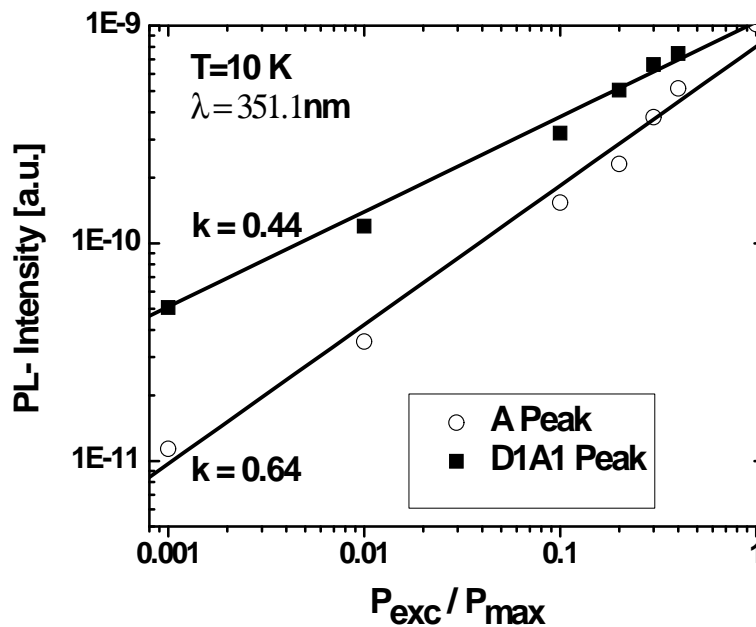

Figure 5.14: *PL spectra of the Ge- Implanted CuGaSe₂ thin films using three kinetic energies, at 10 K and 20 mW using two different excitation line of the Ar⁺ laser at 351.1 nm and 514.5 nm. The UV spectrum is normalized by a 9.83 factor.*

Figure 5.15 displays the power dependence of UV PL spectra measured at 10 K for excitation intensities ranging from 50 mW to 0.05 mW. The k-values of the new emission A at 1.47 eV and of the transition D1A1 are determined to be 0.44 and 0.64 using equation 5.7, i.e. $k < 1$, which is characteristic for a defect correlated recombination mechanism such as free-to-bound or donor- acceptor recombination [82]. In addition the new emission A at 1.47 eV shifts to lower energies as the excitation intensity is reduced by 1.7 meV/ decade. This dependence is characteristic of the donor- acceptor pair (DAP) recombination.
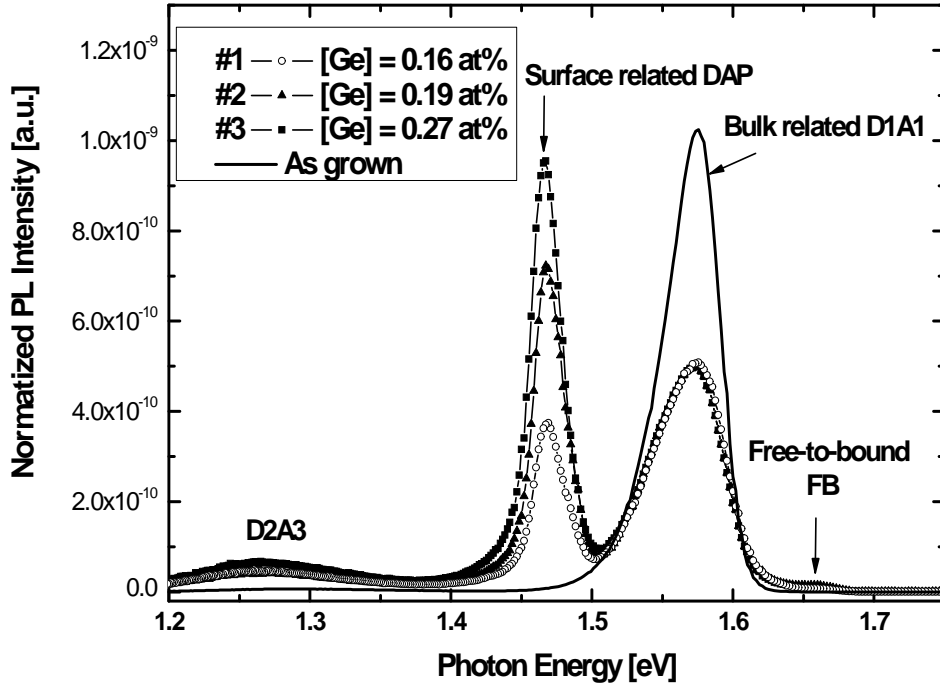
(a)

(b)

Figure 5.15: *(a) PL intensity dependence on excitation for the A and D1A1 transition lines at 10K, and (b) Fitting of the Dependence of PL intensity with excitation intensity*

density P_{exc}/P_{max} using equation 5.7. The k- values are determined from equation 5.7.

Figure 5.16 shows the PL spectra of the Ge- doped CuGaSe$_2$ films recorded after the annealing process for different Ge concentrations determined by SNMS. The intensity of the PL emission at 1.47 eV is normalized to the intensity of the well- known D1A1 line. The PL line at 1.47 eV is the dominant feature in the spectrum at the low energy side and its intensity increases as the Ge concentration increases, thereby the line at 1.47 eV can be related to the implantation of Ge. It worthwhile mentioning that in the reference as- grown and annealed films, this emission was not observed, revealing the sensitivity of the incorporation of Ge into the films.

Figure 5.16: *Photoluminescence of as grown and Ge- doped CuGaSe$_2$ (table 5.1) as a function of Ge atomic concentration($T = 10K$, $\lambda = 351.1$ nm, excitation power of the laser $P = 20$ mW)*
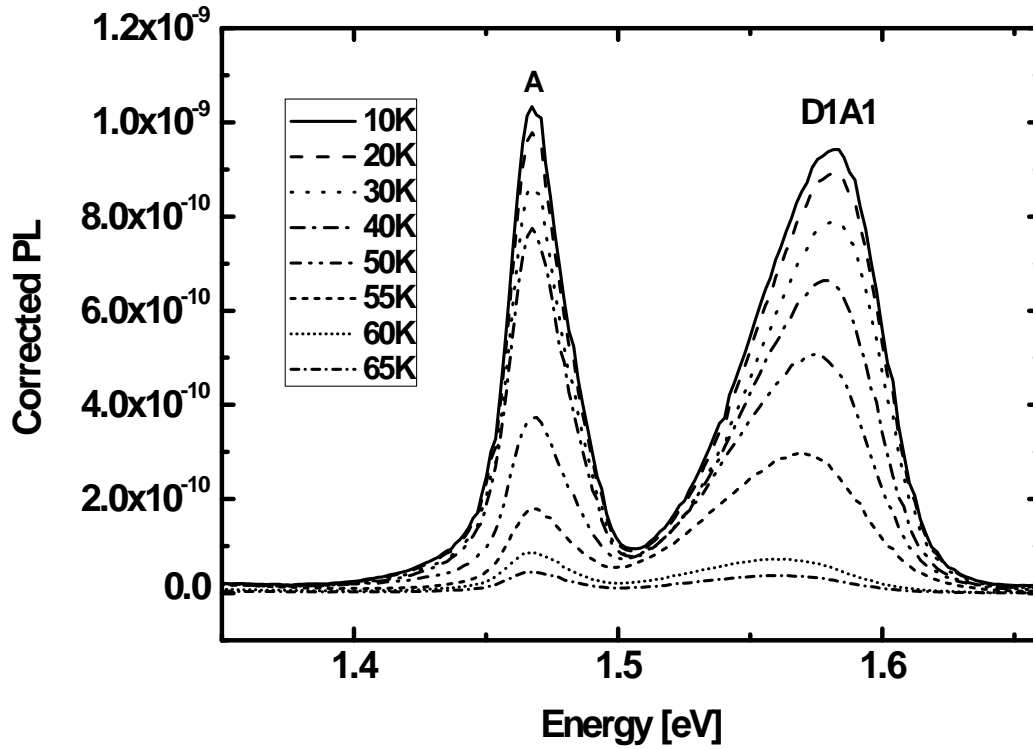
5.4.4 Temperature dependence of peak at 1.47 eV

The emission at 1.47 eV has been observed for the first time only in Ge- doped CuGaSe$_2$ films, therefore this emission is believed to be related to transitions involving Ge- produced defects in the lattice. Figure 5.17 shows the plot of the integrated PL intensity of the 1.47
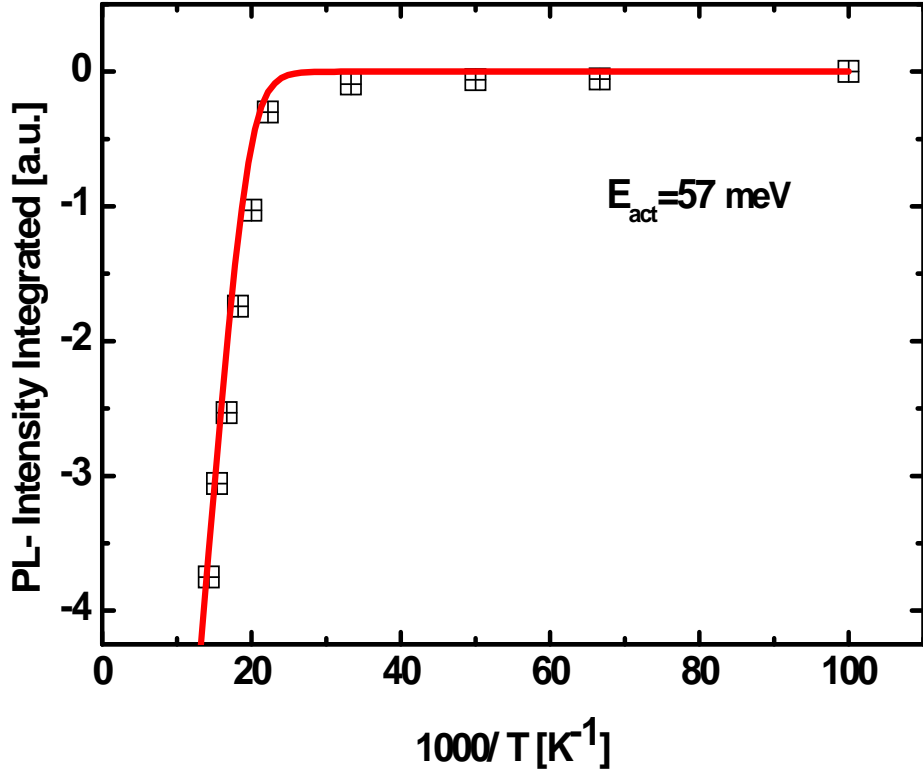
eV emission as a function of temperature. The temperature dependence of this emission line can be described by [83]:

$$I\left(T\right) = I\left(T=0\right)/\left[1 + C\exp\left(-E_{act}/k_B T\right)\right] \qquad (5.8)$$

over the temperature range of 5 to 80 K, where $I\left(T\right)$ is the intensity as a function of temperature T, C a constant describing the capture of carriers at a center and E_{act} is the thermal activation energy of the quenching process. The peak A at 1.47 eV also shifts towards lower energies with increasing temperature, by 1.92 meV/K. This red shift is suggestive of a donor- acceptor pair (DAP) recombination.
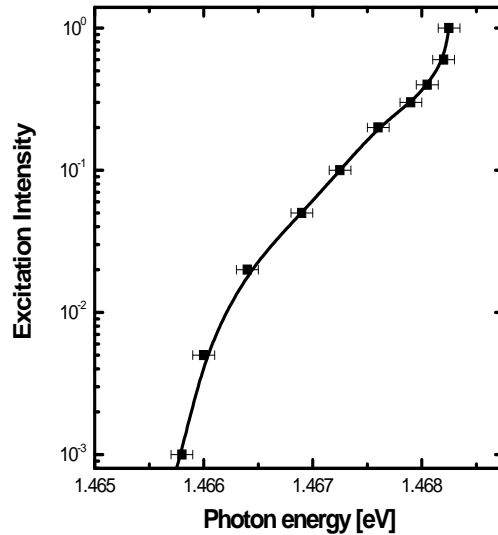

(a)

(b)

Figure 5.17: *(a) Temperature dependence of the UV luminescence of the Ge implanted CuGaSe₂ films (sample 3#) and (b) temperature dependence of the integrated intensity of the 1.47 eV emission. The curves display the results of parameter fitting to equation 5.8 in the temperature range of 10 to 300 K, where the thermal activation energy is estimated to be $E_{act} = 57 \pm 10$ meV. ($\lambda = 351.1$ nm, excitation power of the laser $P = 20mW$).*

The thermal quenching curve shown in figure 5.17 (b) for the emission at 1.47 eV reveals the existence of one energy level with an activation energy of $E_{act} = 57 \pm 10$ meV. However, defect energy levels with the same value have been already found in undoped CuGaSe₂ material for the energy level of the first acceptor A_1 with energy level $E_{A_1} = 60$ meV. Hence, the corresponding defect is believed to be an intrinsic one, namely the copper vacancy, V_{cu} [73]. The sum of the activation energies of the donors and acceptors involved in the 1.47 eV emission has been evaluated by fitting the energy dependence of the emission at 1.47 eV with the excitation intensities using equation 5.4 and is shown in figure 5.18. The fitting parameters are summarized in the table 5.4.

Figure 5.18*: Fit of equation 5.4 to experimental data for the emission line at 1.47 eV in Ge implanted CuGaSe$_2$ films. The line represents the fitting parameters hv_∞ and hv_B.*

Table 5.4: *Fitting parameters hv_∞, hv_B and the sum of the ionization energies of donor and acceptor levels $E_A + E_D$ as derived from the equation 5.3 with the band gap at T =10K, E_g =1.73 eV.*

Defect position	hv_∞ (eV)	hv_B (eV)	E_B (meV)	R_B (Å)	$E_A + E_D$ (meV)
1.47 eV	1,313 ±0.01	1,427±0.01	113.7±10	11.47	417±10

The sum of the activation energy of the donors and acceptors in the 1.47 eV emission is determined to be

$$E_A + E_D = 417 \pm 10 \text{ meV} \tag{5.9}$$

Taking into account the activation energy of the acceptor level $E_{A_2} = 57 \pm 10$ meV, determined by temperature quenching, the activation energy of the donor can be determined from equation 5.9 to be $E_D = 360 \pm 10$ meV. The emission at 1.47 eV stems from transitions between native defects and Ge implantation- induced ones.

5.5 Concluding remarks:

Assuming that the transition D1A4 at 1.64 eV is a donor- acceptor recombination, we have been able to determine the energy level of the acceptor ($E_A = 134\pm10$ meV) and the donor ($E_D = 14\pm10$ meV) involved in this transition using the dependence of the excitation intensity with the corresponding peak position. There is a good agreement between these determined values and the reported ones [76].

The evolution of the CuGaSe$_2$ defect structure has been monitored by means of photoluminescence spectroscopy. A consistency between the defect structure profile with:

- The CCSVT process stages
- The structural properties of the films investigated by EDX, TEM and ERDA (chapter 3) and with the data reported by Klenk *et al* [84] on CuGaSe$_2$ samples prepared by RTP,

has been made, showing that there is a Ga accumulation towards the substrate for CCSVT films deposited directly onto soda lime glass (SLG) as well as for films prepared on Mo-coated SLG structures.

Ge ions have been implanted into device grade CCSVT- grown CuGaSe$_2$ thin films. Thermal annealing was performed for short a time after implantation to reduce the ion implantation–induced damage. With threefold energy implantation one obtains an homogeneous Ge profile in the 200 nm below the surface. Two new emissions induced by the Ge- implantation occurring at 1.67 eV and 1.47eV were highlighted by Vis and UV- PL excitations. They were identified as being free-to-bound (FB) and donor- acceptor pair (DAP) recombinations, respectively. The shallow transition C at 1.67 eV has been attributed to a bulk defect, while the deeper emission A at 1.47 eV, only observed by UV excitation, was ascribed to a new surface- related defect. The latter emission can be resolved as radiative recombination of an electron bound to a deep donor with an ionization energy of $E_D = 360 \pm 10$ meV and a hole bound to the native acceptor in CuGaSe$_2$, namely the copper vacancy V$_{Cu}$.